




Identification of an inter-cysteine loop potentially involved in the activity of *Opisthorchis viverrini*-granulin-1

Rozita Takjoo , David T. Wilson , Paramjit S. Bansal, Alex Loukas , Michael J. Smout* , Norelle L. Daly* 

Australian Institute of Tropical Health and Medicine, James Cook University, Cairns, QLD 4878, Australia

***Correspondence:** Norelle L. Daly, norelle.daly@jcu.edu.au; Michael J. Smout, michael.smout@jcu.edu.au. Australian Institute of Tropical Health and Medicine, James Cook University, Cairns, QLD 4878, Australia

Academic Editor: Xuechen Li, The University of Hong Kong, China

Received: January 6, 2023 **Accepted:** April 20, 2023 **Published:** June 30, 2023

Cite this article: Takjoo R, Wilson DT, Bansal PS, Loukas A, Smout MJ, Daly NL. Identification of an inter-cysteine loop potentially involved in the activity of *Opisthorchis viverrini*-granulin-1. *Explor Drug Sci.* 2023;1:172–9. <https://doi.org/10.37349/eds.2023.00012>

Abstract

Aim: Identification of small bioactive regions in proteins and peptides can be useful information in drug design studies. The current study has shown that an inter-cysteine loop of the N-terminal domain of *Opisthorchis viverrini* granulin-1 (*Ov*-GRN-1), a granulin protein from the flatworm liver fluke *Opisthorchis viverrini* which has potent wound healing properties, maintains the bioactivity of the full-length protein.

Methods: Peptides corresponding to the three inter-cysteine loops of the N-terminal domain were produced using synthetic chemistry, and their structures and bioactivities were analyzed using nuclear magnetic resonance (NMR) spectroscopy and cell proliferation assays, respectively.

Results: As expected for such small peptides, NMR analysis indicated that the peptides were poorly structured in solution. However, a seven-residue peptide corresponding to loop 2 (GRN-L2) promoted cell proliferation, in contrast to the other fragments.

Conclusions: The results from the current study suggest that GRN-L2 might be responsible, in part, for the bioactivity of *Ov*-GRN-1, and might be a useful lead molecule for subsequent wound healing studies.

Keywords

Granulin, peptide, oxidative folding, nuclear magnetic resonance spectroscopy, cell proliferation

Introduction

Identification of small bioactive regions in proteins and peptides can be useful in drug design studies, including peptide mimetic [1, 2] and grafting studies [3–7]. Such bioactive peptides might also be drug leads in their own right, as they are likely to be less immunogenic than larger proteins and easier and cheaper to manufacture [8, 9]. One of the unique approaches to produce bioactive peptides is a process referred to as protein “downsizing” [9], where small, bioactive regions of proteins are produced in isolation. Although downsizing is not as effective where dis-continuous regions are involved in bioactivity, there are several examples where this approach has been effective. For example, downsizing C3a, a 77-residue human

© The Author(s) 2023. This is an Open Access article licensed under a Creative Commons Attribution 4.0 International License (<https://creativecommons.org/licenses/by/4.0/>), which permits unrestricted use, sharing, adaptation, distribution and reproduction in any medium or format, for any purpose, even commercially, as long as you give appropriate credit to the original author(s) and the source, provide a link to the Creative Commons license, and indicate if changes were made.



inflammatory protein, resulting in the identification of a tripeptide with the same high potency, functional profile, and specificity of action as the full-length C3a protein, but with higher plasma stability and bioavailability [9].

The downsizing approach has also been effectively applied to the granulin protein *Opisthorchis viverrini* granulin-1 (*Ov*-GRN-1) from the parasitic human liver fluke, *Opisthorchis viverrini*. *Ov*-GRN-1 is a 6 kDa protein that induces angiogenesis and accelerates wound repair [10]. Although *Ov*-GRN-1 has potent wound-healing properties, low yields in recombinant expression have limited its development as a potential wound-healing agent [11], and prompted studies aimed at producing smaller versions with synthetic methods. A truncated form (GRN_{12-35,3s}) corresponding to residues 12–35 was produced using solid-phase peptide synthesis and folded into a relatively well-defined structure containing a β -hairpin with three disulfide bonds [12]. This truncated form of *Ov*-GRN-1 had similar potency to the full-length protein in an *in vivo* wound healing assay [12] and contains two native disulfide bonds and one non-native disulfide bond, based on the full-length granulin disulfide connectivity [13].

GRN_{12-35,3s} is still a relatively large/structurally complex peptide that comprises three inter-cysteine loops. To determine if *Ov*-GRN-1 can be downsized even further, the three inter-cysteine loops of *Ov*-GRN_{12-35,3s}, referred to as GRN-L1, GRN-L2, and GRN-L3, were individually synthesized using solid-phase peptide synthesis. Cysteine residues were included at the N- and C-termini to allow the formation of a disulfide bond to bring the termini in close proximity and form a loop structure. The structures and cell proliferation effects of these peptides were examined.

Materials and methods

Peptide synthesis and purification

Standard solid-phase peptide synthesis methods were used for the synthesis of the truncated granulin peptides. The peptide chains were assembled on 2-chlorotrityl chloride resin (Peptides International, USA, product code RCT-1056-PI) using manual procedures as previously described [13]. Each peptide contained two cysteine residues, and oxidation of these cysteine residues into a disulfide bond was carried out by incubating the peptides in 100 mmol/L ammonium bicarbonate (pH 8.2) for 24 h at room temperature. The pH was checked after dissolution to confirm the solutions were still at pH 8.0. Preparative reversed-phase high-performance liquid chromatography (RP-HPLC) was used to purify the peptides following the oxidation reaction (Phenomenex Jupiter C18, 10 μ m, 300 Å, 250 mm \times 21.2 mm), and the purity assessed using analytical RP-HPLC (Phenomenex Jupiter 4 μ m Proteo column C12, 10 μ m, 90 Å, 150 mm \times 2 mm). A 1% gradient was used to monitor the purity (0–60% solvent B over 60 min with a flow rate of 0.4 mL/min) and the absorbance was monitored at 214 nm and 280 nm. A 5800 MALDI TOF/TOF mass spectrometer (SCIEX, Framingham, MA, USA) and an LCMS-2020 (Shimadzu, Japan) were used to analyze the masses of the fractions.

Nuclear magnetic resonance spectroscopy and structure calculations

The three-dimensional structures of the peptides were analyzed using nuclear magnetic resonance (NMR) spectroscopy data and calculations based on torsion angle dynamics. Peptides were dissolved at a concentration of \sim 0.2 mmol/L in 90% H₂O/10% D₂O (v/v), pH 4.5, and 4,4-dimethyl-4-silapentane-1-sulfonic acid (DSS; Cambridge Isotope Laboratories) used as an internal chemical shift reference. A 600-MHz AVANCE III NMR spectrometer (Bruker, Karlsruhe, Germany) was used to record spectra which included TOCSY (80 ms mixing time), NOESY (200–300 ms mixing time), and DQF-COSY experiments. The relaxation delay for the experiments was set to 1 s and the temperature was set to 290 Kelvin (K). TOPSPIN software (Bruker, Billerica, MA, USA) was used to process the data, and CCPNMR [14] was used to analyze and assign the spectra based on established protocols [15]. The program CYANA was used to calculate the three-dimensional structures, using a macro for automated assignment of the non-intra-residue NOEs [16]. Restraints for dihedral angles were predicted by TALOS-N and incorporated into the structure calculations [17]. Distance restraints for the disulfide-bonds were included

in the calculations. Structures were visualized using MOLMOL, a molecular graphics program for displaying and analyzing the three-dimensional structures of molecules [18].

Cell culture

The cell line used for the cell proliferation experiments (human skin normal fibroblast cell line, 1BR.3.GN), was obtained from the European Collection of Authenticated Cell Cultures (ECACC, product code 90020509). The conditions used to culture and maintain the cells are those previously described [13] (i.e. complete media: Dulbecco's Modified Eagle Medium/Nutrient Mixture F-12 (DMEM/F12), 1 × GlutaMAX (Thermofisher, product code 10565042) and 1 × antibiotic/antimycotic (penicillin, streptomycin, and amphotericin B; Thermofisher, product code 15240062), 10% fetal bovine serum (FBS; Thermofisher, product code 12664025) at 37°C and 5% CO₂). A 21-residue peptide was used as the negative control. Cell proliferation assays were done in the presence of low nutrient media: DMEM/F12 as above with 0.5% FBS.

Cell proliferation monitoring in real time using xCELLigence

To monitor the cell proliferation, 1BR.3.GN cells seeded at 5,000 cells per well were grown overnight at 37°C in 150 µL of complete media. Agilent E-plates (Agilent) were used for the assays. The cells were monitored using an xCELLigence SP system (Agilent). This system uses gold microelectrodes, which are integrated into the base of tissue culture plates, to measure electrical impedance. Low-nutrient media was used to wash the cells (three times) and incubate the cells (minimum of 6 h) prior to treatment with peptides. Peptides were quantified based on absorbance measurements at 214 nm and predicted extinction coefficients based on the amino acid compositions [19, 20]. Treatments were prepared at 8.5 × target concentration and added to each well in 20 µL, for a final total volume of 170 µL and 1 × concentration. The pH was checked after dissolution to confirm the solutions were still at pH 7. The cell proliferation experiments were carried out over a period of 5–6 days following treatment with the peptides. The xCELLigence system was used to record cell indexes at intervals of 1 h over this time period. To determine the cell proliferation ratios cell index readings were normalized before peptide treatment.

Statistical analysis

A Brown-Forsythe test was used to determine variance homogeneity. It was not possible to determine if the data displayed a normal distribution because of the limited number of data points. A one-way ANOVA test with Holm-Sidak's multiple comparison corrections was used to compare the cell proliferation rates between treatments at each concentration and the nearest peptide control concentration in GraphPad Prism 9.0.

Results

Design and synthesis of *Ov*-GRN_{12-35_3s} fragments

Three *Ov*-GRN_{12-35_3s} fragments (GRN-L1, -L2, and -L3) were chemically synthesized on a 0.1 mmole scale using fluorenylmethyloxycarbonyl (Fmoc) solid-phase peptide synthesis. In the truncated analogue GRN-L3, Cys III and Cys V were replaced with alanine residues to prevent disulfide bond formation between these residues and enable the formation of the Cys IV to Cys VI disulfide bond present in *Ov*-GRN_{12-35_3s}. The folding yields for GRN-L1, GRN-L2, and GRN-L3 were 25%, 33%, and 30% respectively. The sequences of GRN-L1, -L2, and -L3 are shown in Figure 1. In addition, the locations of the loops related to these three fragments are highlighted on the three-dimensional structure of *Ov*-GRN_{12-35_3s}. Following purification of the peptides with RP-HPLC, the correct masses of the peptides were confirmed using MALDI TOF/TOF and electrospray mass spectrometry (Figure S1). Purified GRN-L1 was very broad despite only displaying one mass. This appears to be related to the additional, minor conformations present, as evidenced in the NMR spectra.

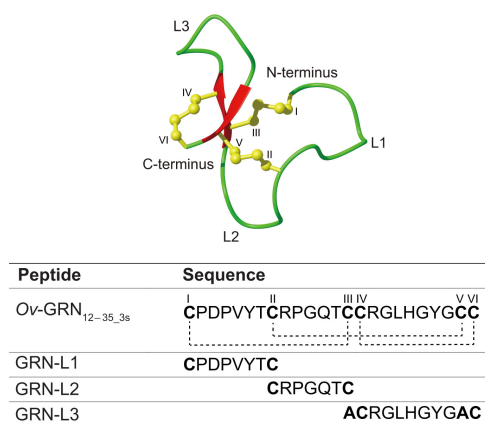


Figure 1. Three-dimensional structure and sequence of Ov-GRN_{12-35_3s}. The sequences of Ov-GRN_{12-35_3s} (PDB ID: 5UJG) and the fragments are given below the structure. The cysteine residues are numbered using Roman numerals (I–VI) and the disulfide bond connections highlighted with dotted lines

Structural analysis with NMR spectroscopy

Analysis of the one-dimensional (Figure 2) and two-dimensional NMR spectra of the truncated granulin peptides allowed the assignment of the majority of the proton resonances and determination of the secondary shifts (Figure 3A). This analysis indicated that the GRN-L1 and -L3 peptides had no consecutive positive or negative secondary chemical shifts, consistent with the peptides being unstructured in solution. The chemical shifts for the Ov-GRN-1 fragments are given in the Table S1. Although GRN-L2 had consecutive positive secondary shifts for residues 4–7, which are consistent with the presence of β -sheet structure, there was a relatively low number of non-intra-residue or sequential NOEs in the NOESY spectrum, which prevented the determination of a well-defined structure. Three-dimensional structures were calculated with CYANA and confirmed the peptides generally had poorly defined structures, albeit constrained by the single disulfide bond as shown in Figure 3B. Structure statistics are given in Table S2. GRN-L2 appears to have the most well-defined structure as a result of having the smallest ring size.

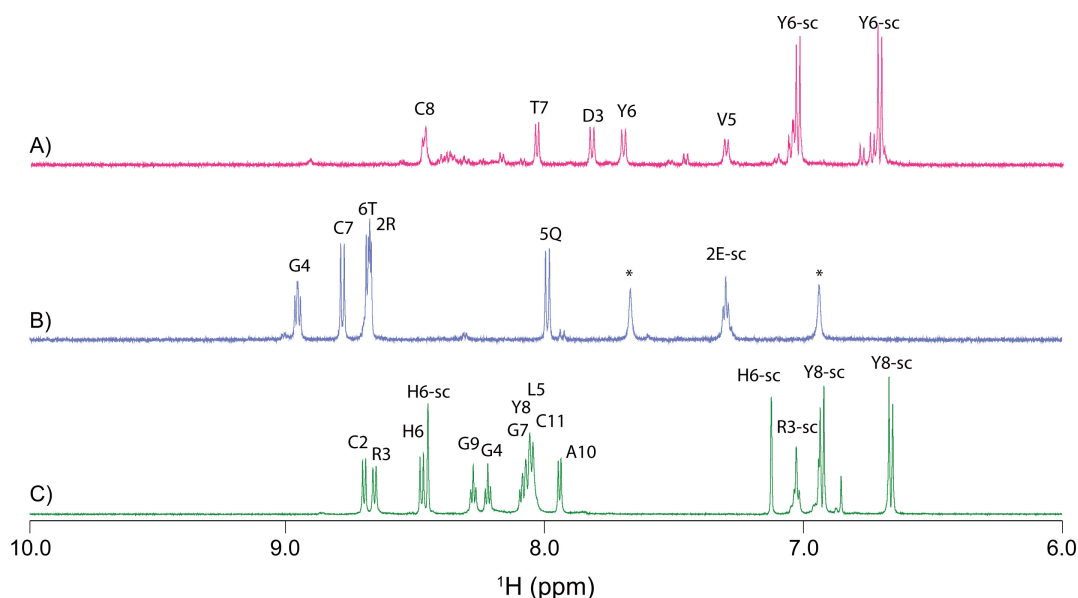


Figure 2. One-dimensional proton NMR spectra of Ov-GRN-1 fragments. A. GRN-L1; B. GRN-L2; and C. GRN-L3. Spectra are shown from 6.5 ppm to 9.5 ppm; this region contains primarily the amide and the aromatic ring protons. Amide protons are labeled with the one-letter code and residue number. Peaks corresponding to side-chain protons are labeled with the one-letter code and residue number and extension -sc. *: NH⁴⁺

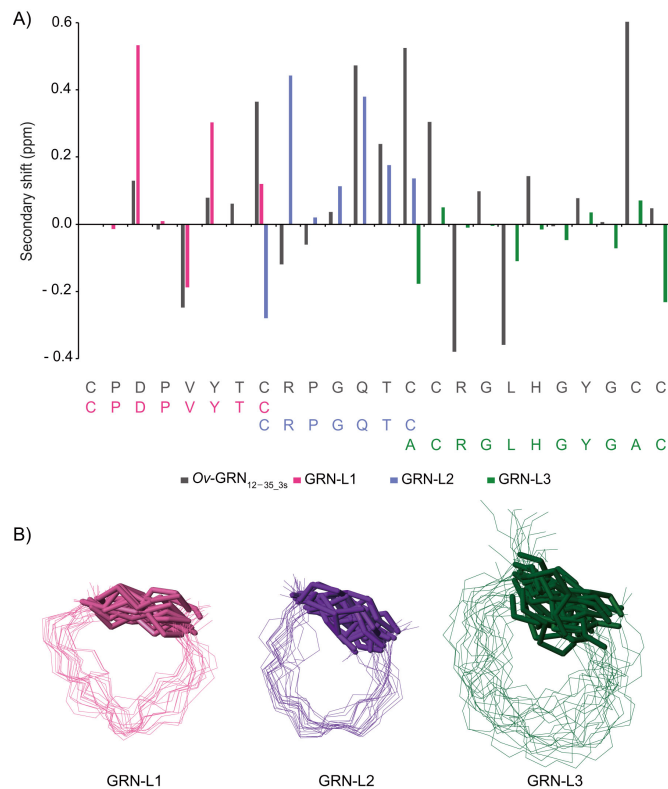


Figure 3. α H Secondary-shifts and three-dimensional representation of *Ov*-GRN-1 fragments. A. The α H secondary shifts were calculated by subtracting the random coil 1 H NMR chemical shifts previously reported by Wishart et al. [21] from the experimental α H chemical shifts. The sequence of the peptides is given at the bottom of the diagram. The *Ov*-GRN_{12-35_3s} (BMRB code: 30232) shifts are provided as a comparison; B. superposition of the 20 lowest energy structures based on CYANA calculations. The disulfide bonds are shown with thickened lines

Cell proliferation assay

The influence of the *Ov*-GRN_{12-35_3s} fragments on the proliferation of a human normal fibroblast cell line in real time was assessed using xCELLigence technology. GRN-L2 resulted in a 13.6% and 13.7% increase ($P < 0.01$) in cell growth compared to the negative control peptide when applied to cells at concentrations of 200 nmol/L and 1 μ mol/L respectively. A 21-residue tropomyosin fragment was used as a negative control; tropomyosin fragments have previously been shown to have no cell proliferation effects [12, 13, 22]. Importantly, this peptide was produced in the laboratory using the same conditions as the *Ov*-GRN_{12-35_3s} fragments. GRN-L1 and GRN-L3 peptides tested at concentrations of 200 nmol/L and 1 μ mol/L did not display statistically significant cell proliferation compared to the peptide control (Figure 4). GRN-L1 and GRN-L2 were also tested at lower concentrations but the cell proliferation was not statistically significant compared to the control peptide. Data from days 1 to 3 are given in Figure S2. The real-time response of the *Ov*-GRN-1 fragments at 1,000 nmol/L (Figure S3) highlights the enhanced potency of the GRN-L2 compared to the two other fragments.

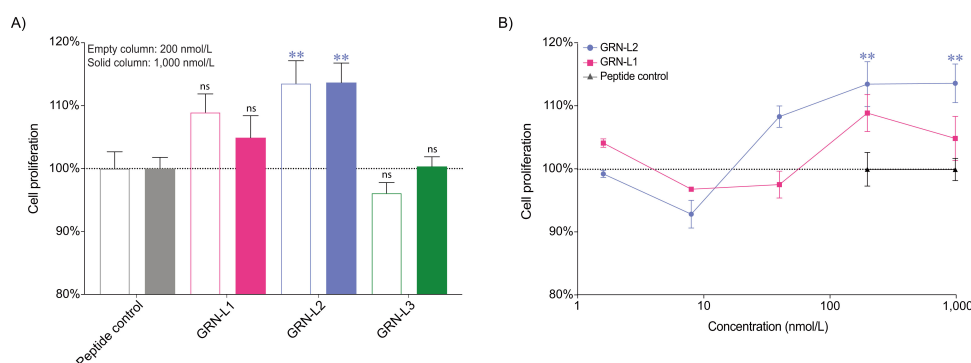


Figure 4. Cell proliferation assay of *Ov*-GRN-1 fragments. The cell index of the fibroblast cell line, 1BR.3.GN, was measured four days after treatment and the proliferation rates relative to peptide control are plotted as mean \pm SEM bars. Data were analyzed by one-way ANOVA against peptide control (ns: not significant, ** $P < 0.01$). A. Empty columns and solid columns represent concentrations of 200 nmol/L and 1 μ mol/L, respectively for the peptide control and *Ov*-GRN-1 fragments. GRN-L2 displayed significant increases in cell proliferation at these two concentrations, in contrast to GRN-L1 and GRN-L3; B. GRN-L1 and GRN-L2 were tested over a wider range of concentrations but significant enhancements in cell proliferation were only observed for the GRN-L2 peptide at 200 nmol/L and 1 μ mol/L. Given the complete lack of activity for GRN-L3 at 200 nmol/L it was not tested at lower concentrations. SEM: standard error of the mean

Discussion

Truncated forms of *Ov*-GRN-1 have significant potential as wound-healing agents but the key features for bioactivity are still poorly understood. In the current study a peptide corresponding to the second inter-cysteine loop of *Ov*-GRN-1 (GRN-L2) was shown to promote cell proliferation of human fibroblasts. This sequence is unique to *Ov*-GRN-1 in the granulin family based on a BLAST search (<https://blast.ncbi.nlm.nih.gov/Blast.cgi>), indicating that this loop could be responsible, in part, for the potent wound-healing activity of *Ov*-GRN-1. The rate of proliferation enhancement is less than the levels observed in previous studies on *Ov*-GRN-1 and truncated *Ov*-GRN-1 peptides [12]. However, further studies are required to determine if this rate of proliferation correlates with wound healing in a mouse model, or ultimately with therapeutic potential in humans.

Based on NMR spectroscopy GRN-L2 appears to be unstructured in solution, suggesting that a well-defined structure is not critical for bioactivity. There are now numerous examples of peptides that lack well-defined structures but still display bioactivity. These examples include disulfide-rich peptides, unstructured because of reduction or modification of the cysteine residues, such as human granulin B and the scorpion venom peptide chlorotoxin (CTX). The structural analysis of fully reduced human granulin B indicated that the peptide was intrinsically disordered, but it was able to induce an inflammatory response in SY-SH5Y human neuroblastoma cells by activation of nuclear factor-kappaB in a concentration-dependent manner [23]. Furthermore, CTX contains 36 amino acids and inhibits glioma cell migration [24]. Despite the full-length peptide having a well-defined structure braced by four disulfide bonds, the reduced form of CTX adopts a random coil structure and inhibits cell migration with a similar potency to CTX [25].

Synthetic fragments of CTX with no disulfide bonds have also been studied and a region corresponding to residues 29 to 36 of CTX, which is not structured in solution, inhibited cell migration, albeit at relatively high concentrations [24]. In a parallel study, this region of CTX was used to design blood-brain barrier shuttles, which included a peptide referred to as miniCTX3, a monocyclic lactam-bridge peptidomimetic containing residues 29–32 of CTX. This truncated analogue of CTX was capable of transporting nanoparticles across endothelial cells [26]. Therefore, the identification of a bioactive, inter-cysteine loop of *Ov*-GRN-1, despite being unstructured in solution, might be useful for further studies in drug design.

Abbreviations

CTX: chlorotoxin

NMR: nuclear magnetic resonance

Ov-GRN-1: *Opisthorchis viverrini* granulin-1

RP-HPLC: reversed-phase high-performance liquid chromatography

Supplementary materials

The supplementary material for this article is available at: https://www.explorationpub.com/uploads/Article/file/100812_sup_1.pdf.

Declarations

Author contributions

NLD: Conceptualization. RT, DTW, MJS, PSB and NLD: Methodology, Investigation, Data curation, Formal analysis. RT and NLD: Writing—original draft. NLD, DTW, PSB and AL: Supervision, Resources. All authors discussed the results and commented on the manuscript.

Conflicts of interest

The authors declare that they have no conflicts of interest.

Ethical approval

Not applicable.

Consent to participate

Not applicable.

Consent to publication

Not applicable.

Availability of data and materials

All datasets for this study are included in the manuscript and the supplementary files.

Funding

RT was supported by a James Cook University PhD scholarship. NLD was supported by a Future Fellowship [110100226]. MJS and AL were awarded by the National Cancer Institute, National Institutes of Health (NIH) [R01CA164719]. The James Cook University NMR facility was partially funded by the Australian Research Council [LE160100218]. The funders had no role in study design, data collection and analysis, decision to publish, or preparation of the manuscript.

Copyright

© The Author(s) 2023.

References

1. Recio C, Maione F, Iqbal AJ, Mascolo N, De Feo V. The potential therapeutic application of peptides and peptidomimetics in cardiovascular disease. *Front Pharmacol.* 2017;7:526.
2. Takata K, Imaizumi S, Kawachi E, Yahiro E, Suematsu Y, Shimizu T, et al. The ApoA-I mimetic peptide FAMP promotes recovery from hindlimb ischemia through a nitric oxide (NO)-related pathway. *Int J Cardiol.* 2016;207:317–25.
3. Swedberg JE, Nigon LV, Reid JC, de Veer SJ, Walpole CM, Stephens CR, et al. Substrate-guided design of a potent and selective kallikrein-related peptidase inhibitor for kallikrein 4. *Chem Biol.* 2009;16:633–43.
4. Chan LY, Gunasekera S, Henriques ST, Worth NF, Le SJ, Clark RJ, et al. Engineering pro-angiogenic peptides using stable, disulfide-rich cyclic scaffolds. *Blood.* 2011;118:6709–17.
5. Poth AG, Chan LY, Craik DJ. Cyclotides as grafting frameworks for protein engineering and drug design applications. *Biopolymers.* 2013;100:480–91.
6. Wang CK, Gruber CW, Cemazar M, Siatskas C, Tagore P, Payne N, et al. Molecular grafting onto a stable framework yields novel cyclic peptides for the treatment of multiple sclerosis. *ACS Chem Biol.* 2014;9:156–63.

7. Conibear AC, Bochen A, Rosengren KJ, Stupar P, Wang C, Kessler H, et al. The cyclic cystine ladder of theta-defensins as a stable, bifunctional scaffold: a proof-of-concept study using the integrin-binding RGD motif. *ChemBioChem*. 2014;15:451–9.
8. Hamley IW. Small bioactive peptides for biomaterials design and therapeutics. *Chem Rev*. 2017;117:14015–41.
9. Reid RC, Yau MK, Singh R, Hamidon JK, Reed AN, Chu P, et al. Downsizing a human inflammatory protein to a small molecule with equal potency and functionality. *Nat Commun*. 2013;4:2802.
10. Smout MJ, Sotillo J, Laha T, Papatpremsiri A, Rinaldi G, Pimenta RN, et al. Carcinogenic parasite secretes growth factor that accelerates wound healing and potentially promotes neoplasia. *PLoS Pathog*. 2015;11:e1005209.
11. Papatpremsiri A, Smout MJ, Loukas A, Brindley PJ, Sripta B, Laha T. Suppression of *Ov-GRN-1* encoding granulin of *Opisthorchis viverrini* inhibits proliferation of biliary epithelial cells. *Exp Parasitol*. 2015;148:17–23.
12. Bansal PS, Smout MJ, Wilson D, Cobos Caceres C, Dastpeyman M, Sotillo J, et al. Development of a potent wound healing agent based on the liver fluke granulin structural fold. *J Med Chem*. 2017;60:4258–66.
13. Takjoo R, Wilson D, Bansal PS, Loukas A, Smout MJ, Daly NL. Folding of truncated granulin peptides. *Biomolecules*. 2020;10:1152.
14. Vranken WF, Boucher W, Stevens TJ, Fogh RH, Pajon A, Llinas M, et al. The CCPN data model for NMR spectroscopy: development of a software pipeline. *Proteins*. 2005;59:687–96.
15. Wüthrich K. NMR studies of structure and function of biological macromolecules (Nobel Lecture)*. *J Biomol NMR*. 2003;27:13–39.
16. Güntert P. Automated NMR structure calculation with CYANA. *Methods Mol Biol*. 2004;278:353–78.
17. Shen Y, Bax A. Protein structural information derived from NMR chemical shift with the neural network program *TALOS-N*. *Methods Mol Biol*. 2015;1260:17–32.
18. Koradi R, Billeter M, Wüthrich K. MOLMOL: a program for display and analysis of macromolecular structures. *J Mol Graph*. 1996;14:51–5.
19. Gill SC, von Hippel PH. Calculation of protein extinction coefficients from amino acid sequence data. *Anal Biochem*. 1989;182:319–26. Erratum in: *Anal Biochem*. 1990;189:283.
20. Hilario EC, Stern A, Wang CH, Vargas YW, Morgan CJ, Swartz TE, et al. An improved method of predicting extinction coefficients for the determination of protein concentration. *PDA J Pharm Sci Technol*. 2017;71:127–35.
21. Wishart DS, Bigam CG, Holm A, Hodges RS, Sykes BD. ¹H, ¹³C and ¹⁵N random coil NMR chemical shifts of the common amino acids. I. Investigations of nearest-neighbor effects. *J Biomol NMR*. 1995;5:67–81.
22. Dastpeyman M, Bansal PS, Wilson D, Sotillo J, Brindley PJ, Loukas A, et al. Structural variants of a liver fluke derived granulin peptide potently stimulate wound healing. *J Med Chem*. 2018;61:8746–53.
23. Ghag G, Wolf LM, Reed RG, Van Der Munnik NP, Mundoma C, Moss MA, et al. Fully reduced granulin-B is intrinsically disordered and displays concentration-dependent dynamics. *Protein Eng Des Sel*. 2016;29:177–86.
24. Dastpeyman M, Giacomini P, Wilson D, Nolan MJ, Bansal PS, Daly NL. A C-terminal fragment of chlorotoxin retains bioactivity and inhibits cell migration. *Front Pharmacol*. 2019;10:250.
25. Ojeda PG, Chan LY, Poth AG, Wang CK, Craik DJ. The role of disulfide bonds in structure and activity of chlorotoxin. *Future Med Chem*. 2014;6:1617–28.
26. Díaz-Perlas C, Varese M, Guardiola S, García J, Sánchez-Navarro M, Giralt E, et al. From venoms to BBB-shuttles. MiniCTX3: a molecular vector derived from scorpion venom†. *Chem Commun*. 2018;54:12738–41.